CELL BIOLOGY

TrpA1 is a shear stress mechanosensing channel regulating intestinal stem cell proliferation in *Drosophila*

Jiaxin Gong[1]†, Niraj K. Nirala[2]†, Jiazhang Chen[3], Fei Wang[1], Pengyu Gu[1], Qi Wen[3], Y. Tony Ip[2]*, Yang Xiang[1]*

Adult stem cells are essential for tissue maintenance and repair. Although genetic pathways for controlling adult stem cells are extensively investigated in various tissues, much less is known about how mechanosensing could regulate adult stem cells and tissue growth. Here, we demonstrate that shear stress sensing regulates intestine stem cell proliferation and epithelial cell number in adult *Drosophila*. Ca^{2+} imaging in ex vivo midguts shows that shear stress, but not other mechanical forces, specifically activates enteroendocrine cells among all epithelial cell types. This activation is mediated by transient receptor potential A1 (TrpA1), a Ca^{2+}-permeable channel expressed in enteroendocrine cells. Furthermore, specific disruption of shear stress, but not chemical, sensitivity of TrpA1 markedly reduces proliferation of intestinal stem cells and midgut cell number. Therefore, we propose that shear stress may act as a natural mechanical stimulation to activate TrpA1 in enteroendocrine cells, which, in turn, regulates intestine stem cell behavior.

INTRODUCTION

Tissue maintenance involves resident stem cells that provide regenerative capacity to replenish lost cells due to aging or damage (*1*, *2*). Intestine is one of the most active regenerative tissues in the human body because of a high rate of cell turnover (*3*, *4*). In mammalian intestines, at least two populations of intestinal stem cells (ISCs) that have different proliferation rates serve to provide progenitors for routine tissue maintenance and damage-induced regeneration (*5*, *6*). This multifaceted regenerative system allows rapid adaptive growth of the mammalian intestine in response to change of food intake or daily assault of ingested substances (*3*, *4*). The regulation of ISC division is therefore essential to maintain the integrity of intestinal epithelia that is tightly linked to the health and survival of an individual (*3*, *7*).

The midgut of adult fruit fly, *Drosophila melanogaster*, contains resident ISCs that serve as the major dividing cells for intestinal tissue homeostasis (*3*, *4*, *8*). Approximately, a thousand ISCs are distributed individually and evenly along the midgut epithelium (*9*, *10*). The midgut epithelium, similar to the mammalian intestine, is largely a single layer of mature enterocytes (ECs) that contain tight junctions to provide both absorptive and barrier functions. ISCs, precursor cells called enteroblasts (EBs), and enteroendocrine cells (EEs) are smaller cells that situated closer to the basal side of the midgut epithelium and serve to support various functions of the intestine (*3*, *4*, *8*). The coordination of ISC division, EB differentiation, and physiological functions of EEs and ECs requires many genetic and signaling pathways that are evolutionarily conserved (*2*, *4*, *8*, *11*). The investigation of these pathways in the adult *Drosophila* midgut as a model organism has provided important insights into intestinal regeneration and tissue wellness in mammalian systems (*2*, *4*, *8*, *11*).

Regulation of ISC activity and intestinal maintenance involves physiological signals such as growth factors, hormones, and innervation of the nervous system, as well as external signals from interaction with commensal and ingested microbes, and ingested food particles and fluids (*2*, *4*, *8*, *11*). The intestinal epithelium is wrapped around by visceral muscle, and the rhythmic peristalsis propels ingested food particles and fluid down the gut lumen. While there is presumed mechanosensing processes, e.g., stretch and shear stress, caused by food particles and fluid passing through the intestinal lumen, the detailed mechanisms of mechanosensing in the gut epithelium and how that may regulate intestinal tissue growth are just beginning to be found (*12*–*19*). Here, we show that a member of the Ca^{2+}-permeable transient receptor potential (Trp) channels family, *Drosophila* TrpA1, a polymodal sensory ion channel that is known to be activated by heat and noxious chemicals and is involved in mechanical nociception (*20*–*25*), mediates shear stress sensing of EEs to indirectly regulate ISC activity and intestine growth.

RESULTS

EE-specific responses to shear stress ex vivo

Shear stress, stretch, and compression are natural mechanical forces produced by gut peristalsis and passing of food and fluid (Fig. 1A). We set out to determine how epithelial cells in the *Drosophila* midgut respond to these mechanical forces using an ex vivo preparation. Because mechanical responses are often associated with elevation of cytosolic Ca^{2+} signals (*26*–*28*), we measured mechanical responses by the genetically encoded Ca^{2+} indicator GCaMP6s (*29*). To stimulate epithelial cells with shear stress, the dissected midgut was placed in a custom-made microfluidic chamber, and the posterior midgut was cut open to expose epithelial cells from the lumen side (fig. S1, A and B). A pump was then connected to

[1]Department of Neurobiology, University of Massachusetts Medical School, Worcester, MA 01605, USA. [2]Program in Molecular Medicine, University of Massachusetts Medical School, Worcester, MA 01605, USA. [3]Department of Physics, Worcester Polytechnic Institute, Worcester, MA 01609, USA.
*Corresponding author. Email: yang.xiang@umassmed.edu (Y.X.); tony.ip@umassmed.edu (Y.T.I.)
†These authors contributed equally to this work.

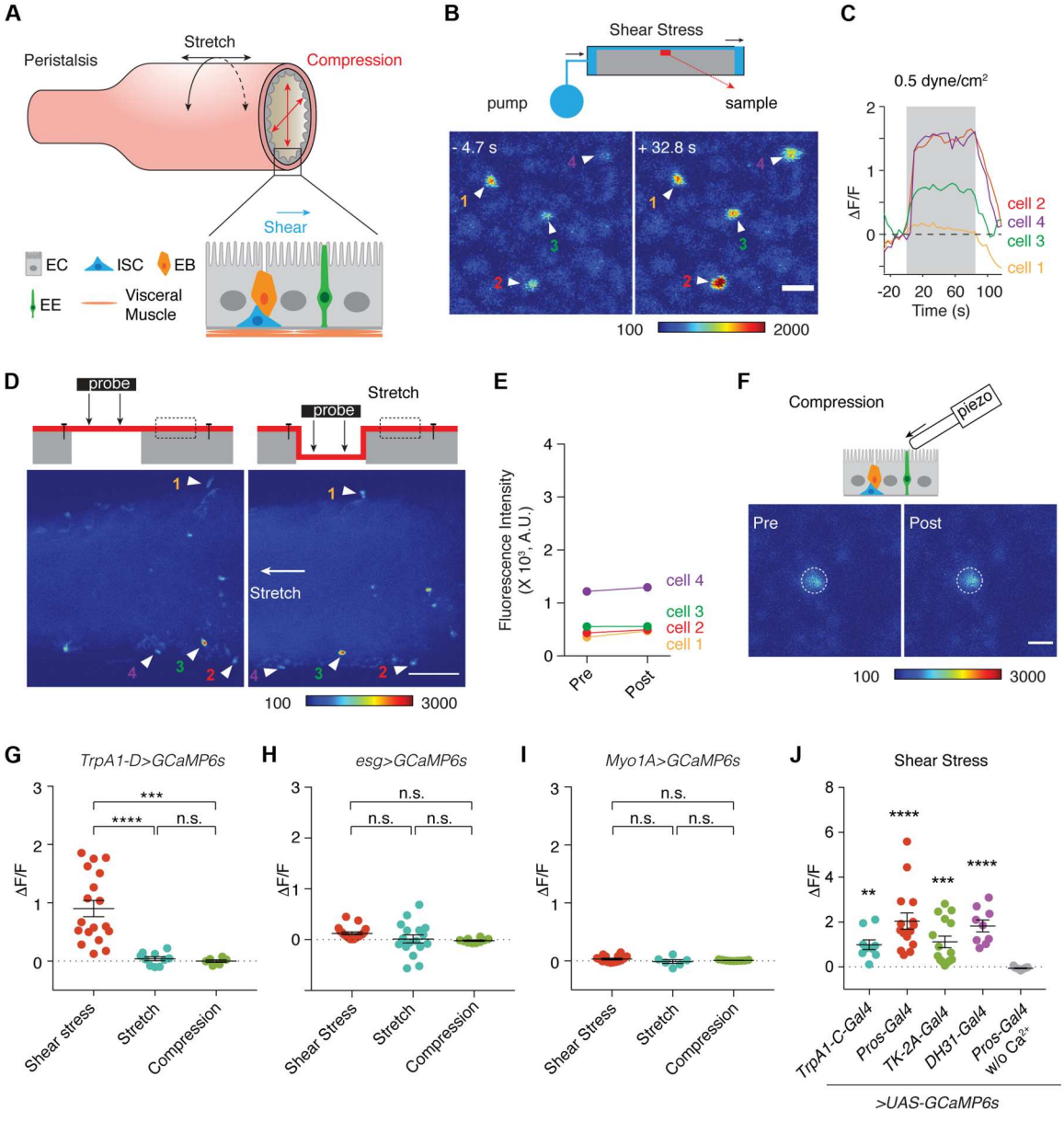

Fig. 1. Shear stress activates adult *Drosophila* midgut enteroendocrine cells (EEs). (**A**) Schematics showing fly midgut cell types and three force types: shear stress, stretch, and compression associated with peristalsis. (**B**) GCaMP responses of posterior midgut EEs before (– shear stress) and during (+ shear stress) shear stress stimulation. Scale bar, 10 μm. Shear stress is delivered to midgut lumen in a microfluidic chamber. (**C**) Ca^{2+} signal traces of EEs from (B) in response to shear stress stimulation (grey region). (**D**) Ca^{2+} signals of EEs before (left) and after (right) stretch. A probe pushed down the fixed posterior midgut toward a cavity as shown in cartoon to cause elongation and stretch of the midgut, and cells in the boxed region over the substrate were imaged by GCaMP. Corresponding EE cells before and after stretch were denoted by arrowheads. Stretch increased distance among cells 2, 3, and 4. Scale bar, 25 μm. (**E**) GCaMP intensity before and after stretch for EEs marked in (D). A.U., arbitrary units. (**F**) A representative EE shows no response to 10-μm compression. The lumen side of the posterior midgut was exposed and stimulated by a fire polished glass probe (~10 μm in tip diameter) that was mounted on a piezo actuator. Scale bar, 5 μm. (**G** to **I**) Quantification of response of EEs (G), intestinal stem cells (ISCs)/enteroblasts (EBs) (H), and enterocytes (ECs) (I) to shear stress, stretch, or compression stimulations. $n \geq 6$ cells. (**J**) Shear stress responses of EEs labeled by other drivers. The group of *Pros-Gal4* in Ca^{2+} free condition (fifth column from left) served as control and was compared to others. $n \geq 9$ cells. One-way analysis of variance (ANOVA) with Dunn's multiple comparisons test. $^{**}P < 0.01$; $^{***}P < 0.001$; $^{****}P < 0.0001$; n.s., not significant.

the microfluidic chamber to deliver laminar flow (Fig. 1B and fig. S1A). Here, the flow rate is positively correlated with the magnitude of shear stress (Fig. 1B) (see Materials and Methods). The shear stress magnitude in the human gastrointestinal tract has been estimated to be up to 30 dyne/cm^2 (*19*, *30*, *31*). Unless specified, we stimulated the *Drosophila* midgut epithelium with a shear stress strength of 0.5 dyne/cm^2, which is likely within the physiological range. Moreover, to measure stretch responses of the midgut, we pushed down a section of intact midgut over a cavity and measured Ca^{2+} responses of cells in a neighboring region (Fig. 1D and fig. S1D). Tissue stretching was evidenced by increased distance between epithelial cells along the anterior-posterior axis (Fig. 1D). Last, we provided compression stimulation of the midgut by direct pushing of the exposed midgut epithelium with a fire polished glass

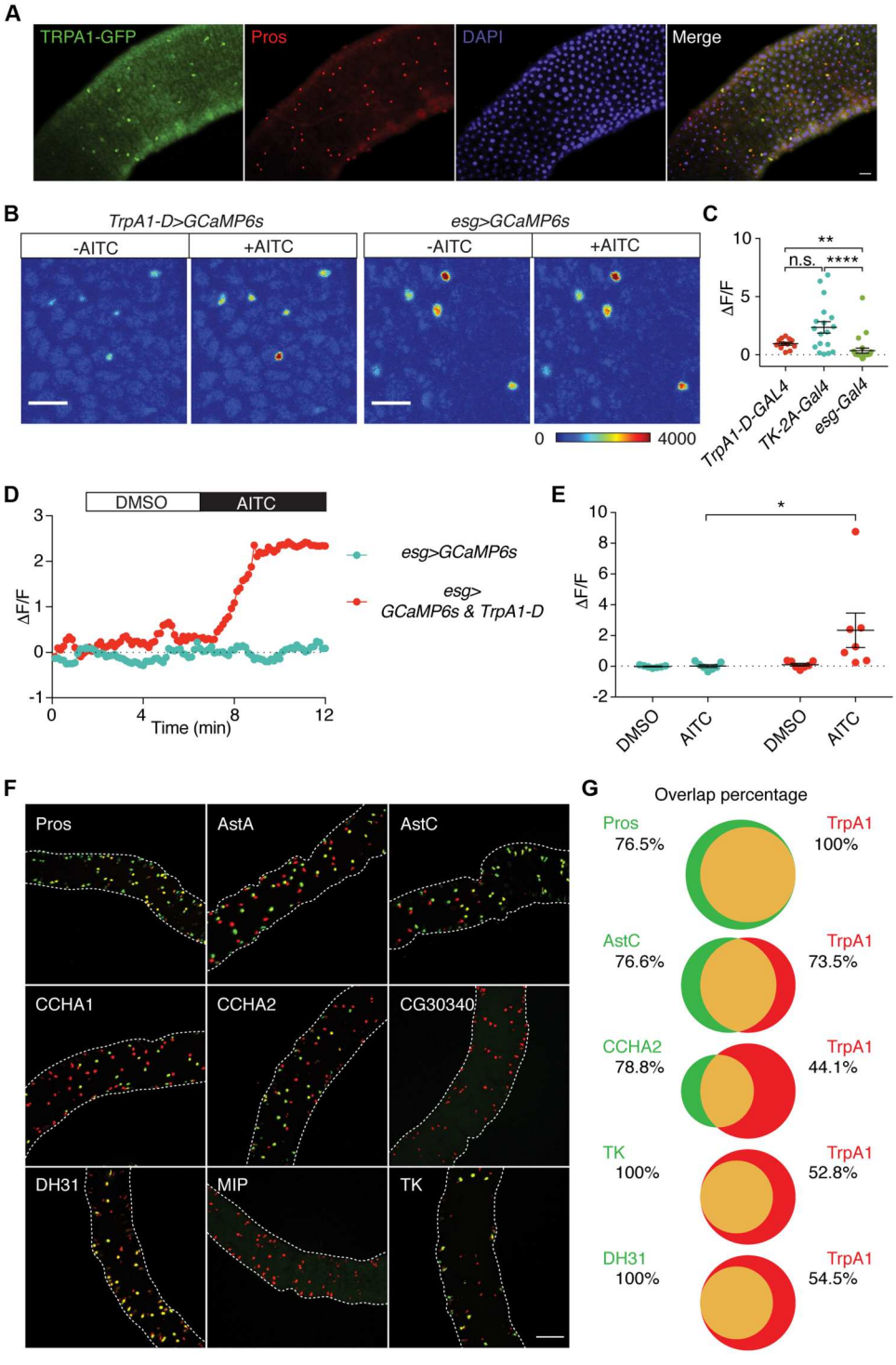

Fig. 2. Expression of transient receptor potential A1 (TrpA1) in midgut enteroendocrine cells (EEs). (**A**) Costaining of green fluorescent protein (GFP) and pan-enteroendocrine cell (EE) marker Pros in *TrpA1-GFP* knock-in flies. Scale bar, 20 μm. DAPI, 4′,6-diamidino-2-phenylindole. (**B**) Representative Ca^{2+} responses to 100 μM TrpA1 agonist allyl isothiocyanate (AITC) of EEs (*TrpA1-D>GCaMP6s*) in posterior midguts. In intestinal stem cells (ISCs)/enteroblasts (EBs) (*esg>GCaMP6s*), there were spontaneous Ca^{2+} spikes but did not change substantially after AITC stimulation. Scale bars, 25 μm. (**C**) Summary of Ca^{2+} responses to 100 μM AITC of EEs (labeled by *TrpA1-D-Gal4* or *TK-2A-Gal4*) and ISCs/EBs (labeled by *esg-Gal4*). $n \geq 12$ cells. One-way analysis of variance (ANOVA) with Dunn's multiple comparisons test. $^{**}P < 0.01$; $^{****}P < 0.0001$. (**D** and **E**) Representative GCaMP imaging traces (D) and summary (E) of ISCs/EBs in posterior midgut with or without expression of a transgenic TrpA1-D isoform, in response to dimethyl sulfoxide (DMSO) (control) and 100 μM AITC. Two-way ANOVA with Bonferroni's multiple comparison test. $^{*}P < 0.05$. (**F**) Expression patterns of TrpA1 and various gut peptides in posterior EEs. Peptide-expressing EEs are labeled by GFP under control of the peptide specific promoter (*peptide-2A-Gal4>UAS-GFP*), and TrpA1-expressing EEs are labeled by mCherry (*TrpA1-2A-LexA>UAS-mCherry*). *Pros-Gal4* is presumably expressed in all EEs. Scale bar, 100 μm. (**G**) Overlap percentage between TrpA1 and Pros, AstC, CCHA2, DH31, or TK. The number specifies the percentage of EEs expressing the gene that also expresses the other gene in the same midgut.

probe mounted on a piezo actuator (Fig. 1F and fig. S1E). To determine responses of each epithelial cell type to shear stress, stretch, and compression, we expressed *UAS-GCaMP6s* under control of various drivers, including *Myo1A-Gal4* for ECs, *esg-Gal4* for ISCs/EBs, and *TrpA1-D-2A-Gal4* for EEs (*10*, *21*, *32*). *TrpA1-D-2A-Gal4*, generated by inserting 2A-Gal4 to the C terminus of *TrpA1* genomic locus in the knock-in allele that expressed only TrpA1-D isoform (*21*), drove expression specifically in EEs in the midgut (see below).

By real-time GCaMP imaging, we found that EEs, but not ECs or ISCs/EBs, of posterior midgut R4-R5 regions quickly responded to shear stress stimulation (Fig. 1, B, C, and G to I). The Ca^{2+} signals of EEs quickly increased and maintained in response to continuous shear stress stimulation (Fig. 1C), indicative of slow adaptation of the shear stress responses. These data indicate that shear stress specifically activates EEs among all midgut epithelial cell types. Shear stress responses of EEs were further confirmed when *UAS-GCaMP6s* was directed by other drivers of EEs, including *prospero (Pros)–Gal4*, *tachykinin (TK)–2A-Gal4*, *DH31-Gal4*, and *TrpA1-C-2A-Gal4* (Fig. 1J) (*21*, *33*–*37*). Removal of external Ca^{2+} (see Materials and Methods) abolished the shear stress response of EEs (Fig. 1J). The threshold for shear stress to activate EEs was between 0.004 and 0.02 dyne/cm^2 (fig. S1C). Unlike shear stress, the other two mechanical stimulations, stretch and compression, did not elicit Ca^{2+} responses in EEs (Fig. 1, D to G), ISCs/EBs (Fig. 1H), or ECs (Fig. 1I) of posterior midgut in these ex vivo assays. Previous reports suggest the involvement of a small population of ISCs/pre-EEs that express Piezo and of EBs that express the Misshapen-Yorkie pathway to be responsive to stretch or food ingestion-associated mechanical stimulation (*13*, *15*). Under our current experimental condition, however, we did not detect mechanical response of these cells. Possible explanations include differences in experimental conditions and the sensitivity of the assays.

TrpA1 expression in EEs

RNA sequencing analysis suggests that only a few Ca^{2+}-permeable channels are expressed in the adult midgut (*38*–*42*). Among them, TrpA1 shows specific expression in EEs, consistent with a previous report showing that pathogen-derived chemicals activate TrpA1 in EEs to modulate defecation (*23*). However, another study suggested that TrpA1 is instead expressed in ISCs/EBs (*22*). To further determine TrpA1 expression in vivo, we used the *TrpA1* knock-in alleles that were generated for fusion of either a green fluorescent protein (GFP) tag or 2A-Gal4 to the C terminus of endogenously expressed TrpA1 protein (*21*). These knock-in alleles reliably report endogenous TrpA1 protein expression in neurons (*21*). Immunostaining in *TrpA1-GFP* knock-in flies revealed that 100% of GFP-positive cells over the whole midgut expressed the EE marker Pros and ~65% of Pros-positive cells expressed TrpA1 (Fig. 2A). As Pros protein staining by the monoclonal antibody used is highly specific in probably all EEs in adult and larval midguts (*9*, *10*), our results indicate that TrpA1 is expressed in a subset of EEs. To assess whether TrpA1 in EEs is functional, we applied the TrpA1 agonist allyl isothiocyanate (AITC), an electrophile chemical found in the pungent spice wasabi that activates TrpA1 through reacting with cysteines (*43*). GCaMP imaging in an ex vivo posterior midgut preparation revealed that acute AITC application activated Ca^{2+} signals in EEs, which were labeled by either *TrpA1-D-2A-Gal4* or *TK-2A-Gal4* (Fig. 2, B and C). In comparison, wild-type ISCs/EBs of posterior midgut did not show Ca^{2+} responses when stimulated by AITC, but only when there was transgenic expression of TrpA1 driven by *esg-Gal4* could these cells respond to AITC stimulation (Fig. 2, B to E), demonstrating that there is no detectable function of TrpA1 normally in these precursor cells. Together, our analyses indicate that TrpA1 is functionally present in EEs, while TrpA1 functions in ISCs/EBs are beyond the detection limit.

EEs express various combinations of over 30 different peptide hormones (*35*, *39*, *44*, *45*). These different EE populations may serve different physiological roles. By using available Gal4 driver lines for some of these hormone genes, we assessed their expression patterns with respect to TrpA1, which was indicated by *TrpA1-2A-LexA* (*21*). The results showed extensive but variable overlap between multiple hormones and TrpA1. Assuming all EEs are labeled by *Pros-Gal4*, TrpA1 was expressed in approximately 75% of all EEs (Fig. 2, F and G). Note that TrpA1-GFP fusion immunostaining data above showed 65% overlap, but Gal4/LexA-driven markers showed higher overlap that is likely due to stronger expression by these driver lines. While expression of many hormones had variable overlap with TrpA1, all TK- and DH31-expressing EEs were TrpA1-positive (Fig. 2, F and G). These results suggest that TrpA1 is expressed in a major population of EEs and that its expression overlaps to a different degree with various gut hormones, which may allow TrpA1 to regulate different physiological functions of the midgut.

EE shear stress sensing depends on TrpA1

The TrpA1 expression pattern suggests a possible role of TrpA1 in shear stress sensing of EEs. To test this possibility, we expressed *UAS-TrpA1-RNAi* in EEs, driven by the *TrpA1-2A-Gal4* driver (*21*). *TrpA1* knockdown led to abolishment of EE responses in posterior midgut to shear stress in the ex vivo preparation (Fig. 3A), indicating that TrpA1 is required for shear stress sensing of EEs to increase intracellular Ca^{2+}. To corroborate this result, we used a null *TrpA1* mutant previously generated in our laboratory that deletes the entire *TrpA1* (*21*) and found that shear stress responses of EEs in posterior midgut were also abolished in this *TrpA1-KO* allele (Fig. 3B). Alternative splicing produced 5 TrpA1 isoforms (fig. S2A). Among them, four isoforms (TrpA1-A, TrpA1-B, TrpA1-C, and TrpA1-D) are functional, whereas the fifth one, TrpA1-E, appears to be functionally dead (*21*). Analysis of expression of individual TrpA1 isoforms using the isoform-specific knock-in alleles revealed that all isoforms were expressed in midgut (fig. S2B) (*21*). When expressed in EEs driven by TK promoter–controlled *R61H07-Gal4*, we found that TrpA1-D, but not TrpA1-A, rescued the shear stress response defect of *TrpA1-KO* flies (Fig. 3B). On the other hand, both TrpA1-D and TrpA1-A rescued the defective responses of EEs to AITC in *TrpA1-KO* (Fig. 3C). Moreover, the E1017K point mutation version of TrpA1-D, which has the channel function abolished (see below), failed to rescue the defective responses of *TrpA1-KO* toward either shear stress or AITC (Fig. 3, B and C). These results indicate that although TrpA1-A and TrpA1-D are both functional in these transgenic rescue assays, TrpA1-D but not TrpA1-A plays a role in EE shear stress sensing. Meanwhile, the mechanosensing channel Piezo as previously reported is expressed in ISCs/pre-EEs (*15*), and our analysis of Piezo mutants did not indicate a function in shear stress sensing of EEs (fig. S3).

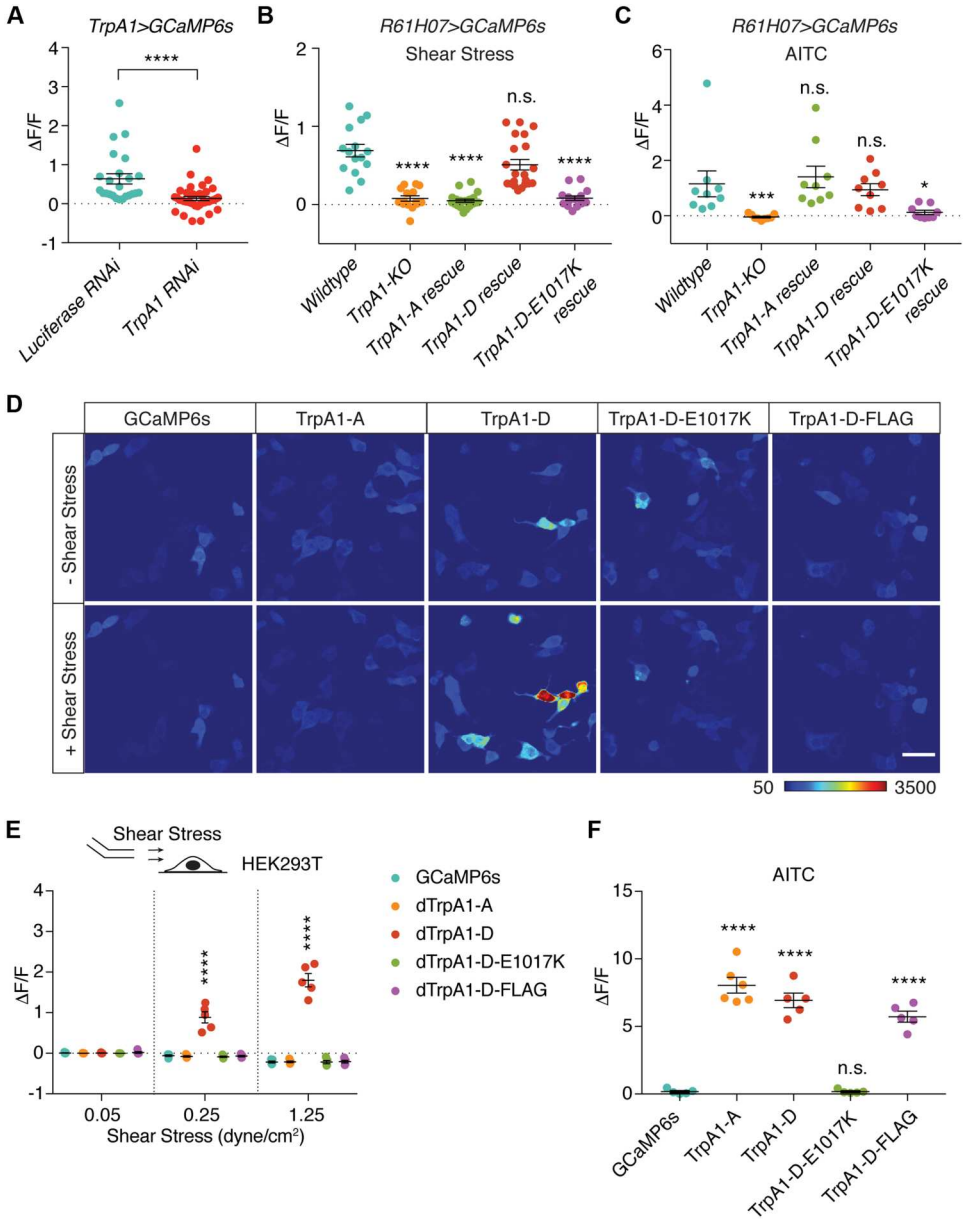

Fig. 3. Transient receptor potential A1 (TrpA1) mediates shear stress responses of enteroendocrine cells (EEs). (**A**) RNA interference (RNAi) knockdown of *TrpA1* suppressed posterior midgut EEs shear stress responses. *Luciferase RNAi* served as control. $n \geq 24$ cells. Two-tailed Mann-Whitney test. ****$P < 0.0001$. (**B** and **C**) Summary of posterior midgut EE responses to shear stress of 0.5 dyne/cm^2 (B) and 100 μM allyl isothiocyanate (AITC) (C) in flies with indicated genotype. The EE-specific driver *R61H07-Gal4* was used to express GCaMP6s and different TrpA1 isoforms. For each group, $n \geq 15$ cells for (B) and $n = 9$ cells for (C). Comparison was made between wild-type and other groups using one-way analysis of variance (ANOVA) with Dunn's multiple comparisons test. *$P < 0.05$; ***$P < 0.001$; ****$P < 0.0001$. (**D**) Representative images showing baseline (− shear stress) and peak (+ shear stress) responses to 1.25 dyne/cm^2, of human embryonic kidney 293 T (HEK293T) cells expressing GCaMP6s alone or together with *Drosophila* TrpA1-A, TrpA1-D, TrpA1-D-E1017K, or TrpA1-D-FLAG. Shear stress was delivered through a micropipette positioned 1 mm away from the center of imaging field. Scale bar, 50 μm. (**E**) Summary of HEK293T cell responses to stepwise shear stress stimulation of 0.05, 0.25, and 1.25 dyne/cm^2. $n = 5$ for each group. Comparison was made between GCaMP6s and other groups using two-way ANOVA with Dunnett's multiple comparisons test. ****$P < 0.0001$. Except for TrpA1-D, no significant differences were found in other groups. (**F**) Summary of HEK293T cell responses to 100 μM AITC. $n \geq 5$ for each group. Comparison was made between GCaMP6s only group and other groups using two-way ANOVA with Dunnett's multiple comparisons test. ****$P < 0.0001$.

Select TrpA1 isoform is shear stress sensitive

To further characterize shear stress responses of TrpA1, we expressed TrpA1-A or TrpA1-D in heterologous cells. GCaMP imaging revealed that human embryonic kidney 293 (HEK293) cells transfected with *Drosophila* TrpA1-D displayed robust Ca^{2+} responses to shear stress delivered through a micropipette, whereas cells expressing TrpA1-A or GCaMP6s alone failed to respond (Fig. 3, D and E). Therefore, select TrpA1 isoform, i.e., TrpA1-D but not TrpA1-A, is shear stress-sensitive. This explains why expression of TrpA1-D but not TrpA1-A could rescue the defective shear stress responses of EEs in *TrpA1-KO* flies (Fig. 3B). Moreover, HEK293 cells transfected with either TrpA1-D or TrpA1-A responded to AITC (Fig. 3F), suggesting that shear stress and electrophiles activate TrpA1 through different mechanisms. Last, HEK293 cells expressing TrpA1-D bearing a point mutation in the putative pore domain (E1017K) responded to neither shear stress nor AITC (Fig. 3, D to F), indicating that ion conduction is essential for TrpA1 to respond to both mechanical and chemical stimuli.

TrpA1 regulates ISC proliferation and intestinal cell number in adult midgut

The adult midgut epithelium consists essentially a monolayer of ECs occupying most of the epithelium, while the smaller-sized ISC/EB precursor cells and EEs are located closer to the basement membrane. The adult midgut epithelium continues to grow, albeit slowly under normal feeding conditions, after eclosion from pupal stage, and the growth is largely supported by the division of ISCs (*46*). As flies age, the midgut epithelium accumulates more cells, and older flies exhibited age-related dysplasia (*47*). We showed that more cells were packed together in the midguts of older w^{1118} control flies, as exemplified by staining of β-catenin that reveals the cell membrane, together with staining of Pros that marks EE nuclei (fig. S4, A and B). We next examined phenotypic changes in *TrpA1-KO* flies and found that, when compared to age-matched w^{1118} control flies, *TrpA1-KO* flies exhibited markedly young-looking midgut epithelia. In *TrpA1-KO* flies, the midgut epithelium appeared morphologically normal, but older mutant midguts resembled young midguts with fewer cells packed together (fig. S4, A and B). Quantification of mitotic activity by the phosphorylated histone 3 (p-H3) staining revealed a markedly reduced cell division especially in older (30- and 40-day-old) *TrpA1* mutant flies when compared to age-matched w^{1118} flies (Fig. 4, A and B). Most of the p-H3 staining in adult midguts likely represents ISC division, although EE division is also possible in older midguts but should represent less than 5% of p-H3 counts (*44*). In addition to the reduced mitotic count, we found that the number of all epithelial cell types including ECs, ISCs/EBs, and EEs was reduced in older *TrpA1* mutant flies (Fig. 4, C to E), suggesting that decreased ISC division after loss of TrpA1 could underlie the reduced overall cell numbers and therefore reduced growth/dysplasia in the adult midgut. In contrast, mitotic counts, as well as the number of ECs and ISCs/EBs were comparable between young (7-day-old) *TrpA1-KO* flies and w^{1118} control flies, although there was a reduction in the number of EEs in *TrpA1-KO* flies (fig. S4, B to D).

In addition to midgut, TrpA1 has been shown to express in neurons (*21*). To further assess the role of TrpA1 in EEs, we combined *Pros-Gal4* with *elav-Gal80*, which produces the Gal4 repressor Gal80 in all neurons under the control of pan-neuronal promoter *elav* (*48*). When this driver was crossed to *UAS-TrpA1-RNAi* to knock down *TrpA1* specifically in EEs, we found that p-H3 counts were also markedly reduced to a degree similar to *TrpA1-KO* flies (Fig. 4F). *TKg-Gal4* has been shown to mainly express in EEs, despite sparse expression in neurons (*36*). Similarly, expression of *TrpA1-RNAi* under the control of *TKg-Gal4* caused substantial reduction in p-H3 counts (Fig. 4G). A previous report suggested that TrpA1 may have an autonomous function in ISCs/EBs. Therefore, we expressed *TrpA1-RNAi* in these precursor cells and did observe some reduction of mitotic counts (fig. S5, A and B). While we cannot exclude some functions of TrpA1 within ISCs/EBs (see Discussion), our results overall indicate that TrpA1 expresses mainly in EEs and has a critical function in EEs to nonautonomously regulate ISC proliferation.

We next tried transgenic rescue experiments of the *TrpA1-KO* flies with *TKg-Gal4* and *UAS-TrpA1* transgenes but observed inconsistent results, possibly due to the findings that TrpA1 overexpression could affect the in vivo functions of the cells (*21*, *49*) or that *TKg-Gal4* might not be able to fully capture the function repertoire of TrpA1 in EEs. Therefore, we turned to isoform specific knock-in alleles that we generated including the *TrpA1-A-KI* and *TrpA1-D-KI* (*21*). These alleles have the *TrpA1* genomic locus modified such that the entire *TrpA1* is deleted and is further replaced by genomic sequences that express only a single TrpA1 isoform (i.e., *TrpA1-A-KI* and *TrpA1-D-KI* express A and D isoforms, respectively). As such, they are loss of function *TrpA1* mutants but with expression of only TrpA1-A or TrpA1-D driven by the endogenous promoter. The *TrpA1-D-KI* flies exhibited consistent mitotic counts that were notably higher than *TrpA1-A-KI* or *TrpA1-KO* flies (Fig. 4H). As TrpA1-D and TrpA1-A differ in their shear stress sensitivity, these results suggest that shear stress sensing of TrpA1 in EEs contributes to ISC proliferation. Notably, the overall midgut proliferation in *TrpA1-D-KI* midguts was lower than that in wild-type flies, suggesting that TrpA1 isoforms other than TrpA1-D could also contribute to regulation of midgut ISCs.

TrpA1 shear stress sensing controls ISC proliferation

In addition to shear stress, *Drosophila* TrpA1 is known to sense heat, as well as irritant chemicals including electrophiles (e.g., AITC) and reactive oxygen species (ROS; e.g., H_2O_2) (*21*, *50*–*52*). As we raised flies at the ambient temperature of ~23°C, which is below the TrpA1 heat-activation threshold (*21*), defective ISC proliferation and midgut cell number observed in *TrpA1-KO* flies are unlikely due to loss of the heat sensing function of TrpA1. Because shear stress, electrophiles, and ROS could be present in gut lumen, delineating the precise role of mechanosensing of EEs requires selective disruption of shear stress, but not chemical, sensitivity of TrpA1. Intriguingly, *TrpA1-FLAG* knock-in flies, which were generated by inserting the FLAG tag to the C terminus of *TrpA1* immediately before the stop codon (*21*), met this requirement. Specifically, shear stress responses of EEs in posterior midgut were abolished in *TrpA1-FLAG* flies, similar to *TrpA1-KO* flies (Fig. 5, A and B). On the other hand, unlike *TrpA1-KO* flies in which EEs lost responses to irritant chemicals, EEs in posterior midgut of *TrpA1-FLAG* flies retained normal responses to H_2O_2 and AITC (Fig. 5, C and D). Furthermore, we have previously shown that heat nociception is intact in *TrpA1-FLAG* flies (*21*). These results together reveal *TrpA1-FLAG* as a desired genetic tool to assess the in vivo function of shear stress sensing of EEs. We found that p-H3 counts in the midgut were markedly reduced

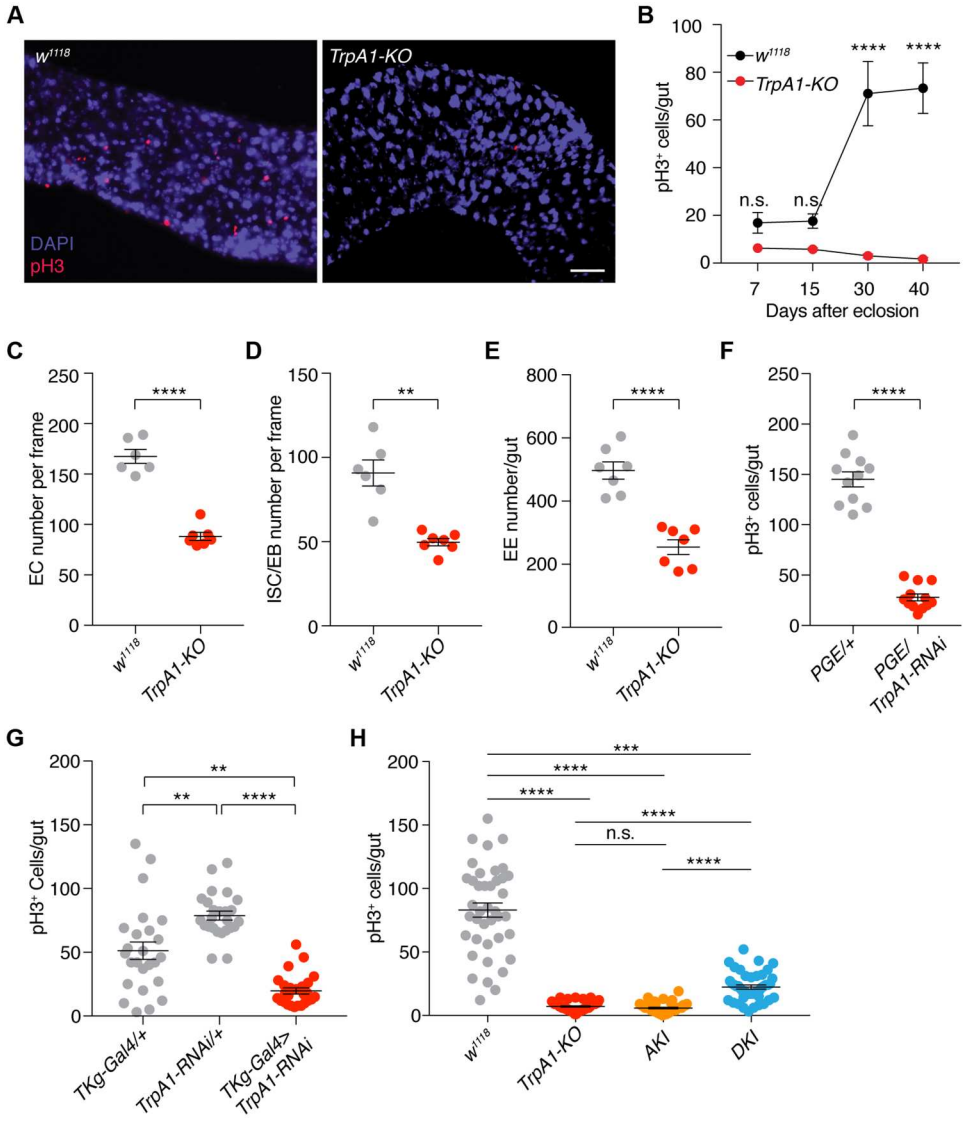

Fig. 4. *TrpA1-KO* flies exhibited reduced dysplasia in aged flies. (**A**) Representative images of phosphorylated histone 3 (p-H3) staining (red) from 30-day-old w^{1118} and *TrpA1-KO* flies. Scale bar, 20 μm. (**B**) Mitotic p-H3$^+$ cell counts from whole midgut at different ages. $n \geq 10$ animals for each group. Two-way analysis of variance (ANOVA) with Bonferroni's multiple comparisons test. ****$P < 0.0001$. (**C** to **E**) Number of enterocytes (ECs) (C), intestinal stem cells (ISCs)/enteroblasts (EBs) (D), and enteroendocrine cells (EEs) (E) in 40-day-old w^{1118} and *TrpA1-KO* flies. $n \geq 6$ animals. Two-tailed Student's *t* test. **$P < 0.01$; ****$P < 0.0001$. (**F**) RNA interference (RNAi) knockdown of *TrpA1* in EEs reduced ISCs proliferation. *Pros-Gal4*, *elav-Gal80* (*PGE*) was used to drive expression of *TrpA1-RNAi* only in EEs but not neurons. Forty-day-old flies were examined. $n \geq 11$ animals. Two-tailed Student's *t* test. ****$P < 0.0001$. (**G**) Mitotic p-H3$^+$ cells count from 40-day-old flies with expression of *UAS-TrpA1-RNAi* driven by *TKg-Gal4*. Total $n \geq 25$ samples for each group. One-way ANOVA with Dunn's multiple comparisons test. **$P < 0.01$; ****$P < 0.0001$. (**H**) Mitotic p-H3$^+$ cell counts from whole midguts of 40-day-old w^{1118}, *TrpA1-KO*, TrpA1-A knock-in (*A-KI*), and TrpA1-D knock-in (*D-KI*) flies. One-way ANOVA with Dunn's multiple comparisons test. ***$P < 0.001$; ****$P < 0.0001$.

in *TrpA1-FLAG* flies (Fig. 5E), providing direct evidence that shear stress sensing of EEs is required for ISC proliferation. Last, we characterized the property of TrpA1-FLAG by expressing FLAG-tagged TrpA1-D (TrpA1-D-FLAG) in heterologous cells. Consistent with our results in EEs, we found that HEK293 cells transfected with TrpA1-D-FLAG failed to respond to shear stress but exhibited robust responses to AITC (Fig. 3, D to F). These findings suggest that the C-terminal integrity is essential for shear stress, but not chemical, sensing of TrpA1.

To assess whether midguts of *TrpA1-KO* or *TrpA1-FLAG* flies could respond to oxidative stress, we fed flies with paraquat, a chemical that stimulates ROS production and promotes ISC proliferation (*22*, *47*, *53*). The results show that paraquat feeding can cause similar increases of ISC proliferation in w^{1118}, *TrpA1-KO*, and *TrpA1-FLAG* flies (fig. S6). The result is also consistent with the fact that paraquat could activate the stress signaling pathways in all midgut epithelial cells to increase ISC proliferation (*47*). Therefore, *TrpA1-KO* and *TrpA1-FLAG* flies are still capable of sensing stress signals to promote ISC proliferation.

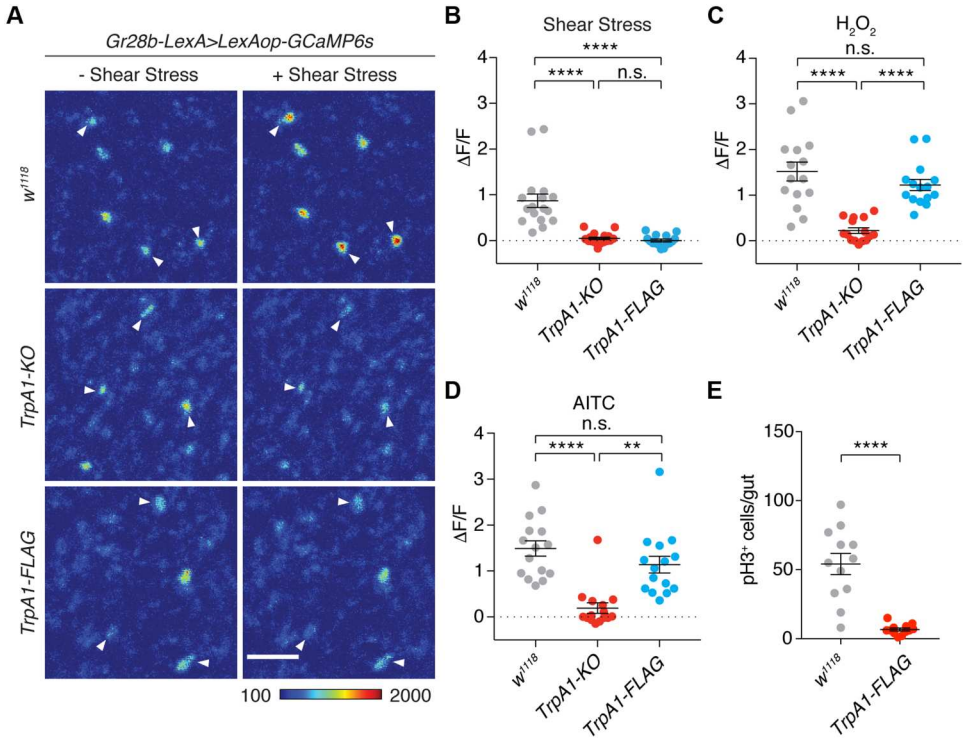

Fig. 5. Transient receptor potential A1 (TrpA1) shear stress sensing function is essential for intestinal stem cell (ISC) proliferation. (**A**) GCaMP images of enteroendocrine cells (EEs) before (− shear stress) and during (+ shear stress) shear stress stimulation of 0.5 dyne/cm^2 from w^{1118} control, *TrpA1-KO*, and *TrpA1-FLAG* fly posterior midguts. EEs are labeled by *Gr28b-LexA>LexAOP-GCaMP6s*. Arrowheads denote representative EE cells. Scale bar, 20 μm. (**B**) Summary of EE responses to shear stress from w^{1118} control, *TrpA1-KO*, and *TrpA1-FLAG* flies. $n \geq 15$ cells. One-way analysis of variance (ANOVA) with Dunn's multiple comparisons test. ****$P < 0.0001$. (**C**) Summary of posterior midgut EE responses to 10 mM H_2O_2 from w^{1118} control, *TrpA1-KO*, and *TrpA1-FLAG* flies. $n = 15$ cells for each group. One-way ANOVA with Tukey's multiple comparisons test. ****$P < 0.0001$. (**D**) Summary of posterior midgut EE responses to 100 μM AITC from w^{1118} control, *TrpA1-KO*, and *TrpA1-FLAG* flies. $n = 15$ cells for each group. One-way ANOVA with Dunn's multiple comparisons test. **$P < 0.01$; ****$P < 0.0001$. (**E**) Mitotic p-H3$^+$ cell count from whole midgut of 40-day-old w^{1118} control and *TrpA1-FLAG* flies. $n = 12$ animals for each group. Unpaired Student's *t* test. ****$P < 0.0001$.

TrpA1 modulates Ca^{2+} oscillation within ISCs to regulate their proliferation

Data presented so far suggest that TrpA1 in EEs can cell nonautonomously regulate ISC proliferation and therefore intestine cell numbers. ISC proliferation is increased in old wild-type flies (Fig. 4B), suggesting a possibility that shear stress sensing by EEs could promote ISC proliferation with age in wild-type flies. To test whether old flies could exhibit stronger midgut peristalsis, we fed wild-type flies of different ages with food containing food dye and estimated peristalsis by measuring movement of the dye in the midgut. The results suggest that peristalsis was comparable for 10, 20, and 40-day-old flies (fig. S7, A and B), arguing that the midgut epithelium of young and old flies is likely exposed to similar mechanical stress. Last, we found that the responses of EEs in posterior midgut to AITC were comparable in 10-, 20-, and 40-day-old flies (fig. S7C), suggesting that TrpA1 activity remains constant in old versus young flies. These analyses suggest that mechanisms other than mechanosensing per se, possibly the effectors of mechanosensing such as signaling between activated EEs and ISCs, could be modulated in old wild-type flies to account for increased ISC proliferation.

Previous reports indicate that Ca^{2+} oscillation within ISCs promotes their proliferation and that multiple cell types in the intestinal epithelium also have Ca^{2+} oscillation (*54*, *55*). When we examined Ca^{2+} signals in ISC/EB cell nests in 20-day-old animals, we found an almost complete loss of Ca^{2+} oscillation in posterior midgut of *TrpA1-KO* flies, when compared with age-matched w^{1118} control (Fig. 6, A and B, and movies S1 and S2). Moreover, Ca^{2+} oscillation within ISCs/EBs was also abolished in posterior midgut of *TrpA1-FLAG* flies (Fig. 6, A and B, and movie S3), implicating a role of shear stress sensing of EEs in Ca^{2+} oscillation in ISCs. Defective Ca^{2+} oscillation was unlikely due to the reduced number of ISCs at this stage of 20 days old, as the number of ISCs/EBs revealed by the *esg-Gal4*–driven nuclear mCherry appeared to be normal in *TrpA1-KO* and *TrpA1-FLAG* flies (Fig. 6A, right panels). Together, our results suggest that shear stress sensing of EEs could regulate Ca^{2+} oscillation within ISCs to control their proliferation.

DISCUSSION

Many tissues in vivo are exposed to complex mechanical environment. However, how mechanosensing could regulate tissue maintenance is not well understood. In this study, we found previously unknown cellular and ion channel mechanisms by which shear stress could control intestine stem cell proliferation and midgut cell number in adult *Drosophila*. As shown in Fig. 6C, food/fluid ingestion and midgut peristaltic contraction likely generate shear stress as a natural stimulus, which we show here is sensed

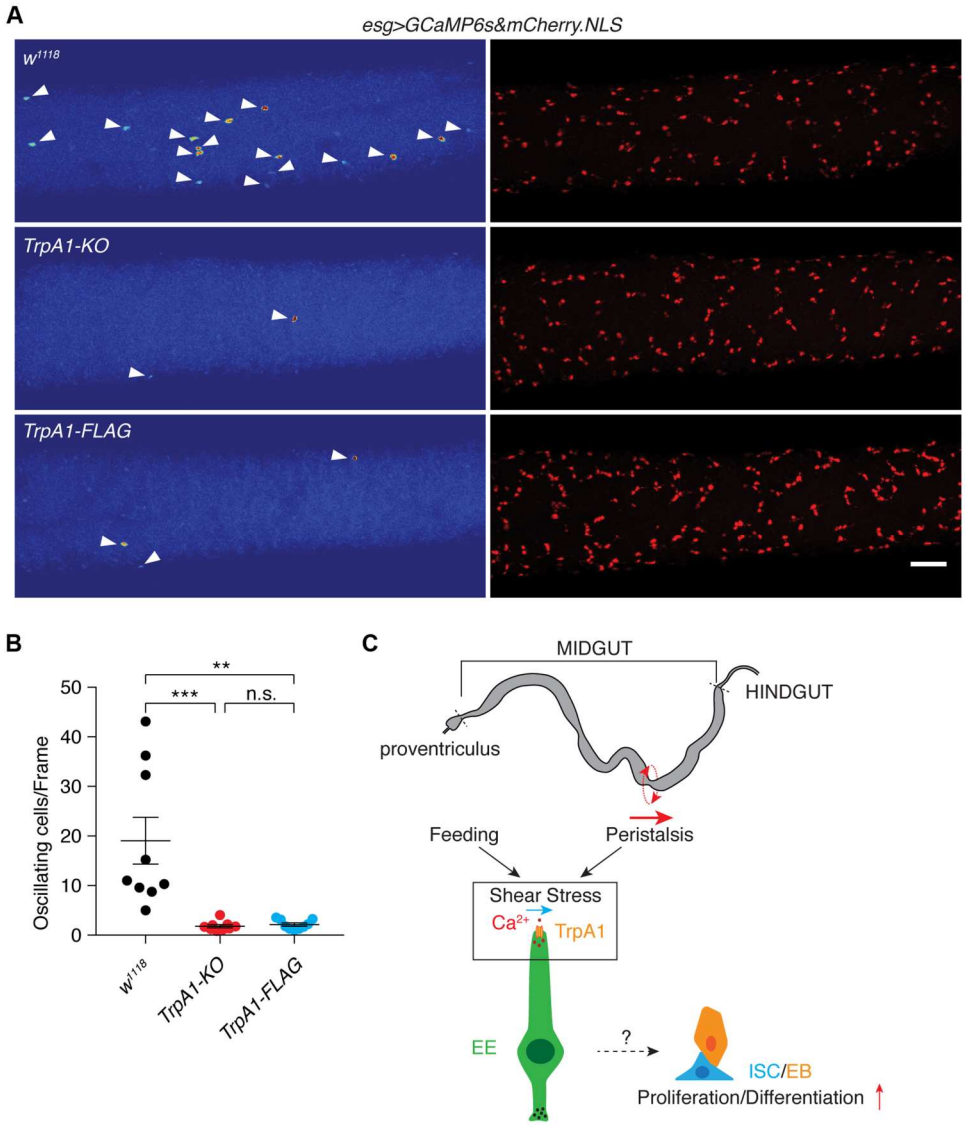

Fig. 6. Transient receptor potential A1 (TrpA1) shear stress sensing regulates Ca^{2+} oscillation in intestinal stem cells (ISCs)/enteroblasts (EBs). (**A**) Sample images of spontaneous Ca^{2+} oscillation (left panels) in posterior midgut ISCs/EBs (*esg-Gal4>UAS-GCaMP6s*) from w^{1118} control, *TrpA1-KO*, and *TrpA1-FLAG* flies. The ISCs/EBs are also labeled by a nuclear marker mCherry.NLS (right panels). Scale bar, 50 μm. (**B**) Number of oscillating cells per frame during 10 min tracking from 20-day-old w^{1118} control, *TrpA1-KO*, and *TrpA1-FLAG* flies. $n \geq 9$ animals. One-way analysis of variance (ANOVA) with Dunn's multiple comparisons test. $^{**}P < 0.01$; $^{***}P < 0.001$. (**C**) A summary of TrpA1 function in adult midgut enteroendocrine cells (EEs), in response to shear stress to control Ca^{2+} signals in EEs and then act through a yet to be understood mechanism that regulates ISC proliferation and/or differentiation. The dashed arrow indicates that EE-derived hormones/peptides could either directly signal to ISCs or indirectly through intermediate cell types.

specifically by EEs through TrpA1. Our findings reveal the mechanosensitive function of TrpA1, in addition to its established roles as a sensor for heat and irritant chemicals. Although TrpA1 respond to both mechanical and chemical stimuli, our findings of reduced mitotic counts in *TrpA1-FLAG* flies, which showed impaired responses of EEs to shear stress but normal responses to irritant chemicals, suggest that mechanosensing of EEs critically controls ISC proliferation.

TrpA1-D but not TrpA1-A confers shear stress responses to EEs in the rescued fly midgut and to HEK293 cells. The sequence difference between these two splicing variants is ~100 amino acids in the N terminus, implicating a role of the N terminus of TrpA1 in mechanosensing. The C terminus also appears to be critical, as shear stress sensing of TrpA1 is abolished after adding the small FLAG tag to the C terminus of TrpA1. It is plausible that interactions of the N and C termini, both facing the cytoplasm, could play a role in mechanosensing. On the other hand, AITC can activate TrpA1-D, TrpA1-A, and TrpA1-FLAG, indicating that chemical sensitivity of TrpA1 requires different structural determinants.

Stretch of the adult *Drosophila* midgut has been shown to activate Piezo in a subset of ISCs/pre-EEs that will differentiate into EEs, to cell-autonomously regulate ISC differentiation (*15*). To test whether Piezo could be involved in shear stress responses, we performed GCaMP imaging and found that responses of EEs to

shear stress were unaffected in *Piezo*^{KO} fly midguts (fig. S3). Therefore, TrpA1, instead of Piezo, is the primary shear stress sensor in *Drosophila* EEs. These results also indicate that multiple forces, including shear stress and stretch, could activate different mechanosensitive ion channels in different epithelial cell types, to orchestrate ISC behavior and adaptive growth of the *Drosophila* midgut.

Two previously published papers suggested different expression and function of TrpA1 either in EEs (*23*) or in ISCs/EBs (*22*). The use of *esg-Gal4* as a driver of *TrpA1-RNAi* for loss of function studies in ISCs/EBs (*22*) still allows alternative interpretations, because this driver has expression in a small number of EEs in middle midgut (*39*). We noted overlapped expression between *esg-Gal4* and *TrpA1-T2A-LexA* in a few cells in middle midgut (fig. S5C). Moreover, ISCs naturally divide and differentiate into EEs, and the RNA interference (RNAi) driven by *esg-Gal4* may linger into newborn EEs. Our own investigation using the *esg-Gal4*–driven *TrpA1-RNAi* revealed variable results of midgut proliferation under different conditions (fig. S5, A and B), which underscore the importance of the use of multiple drivers and genetic approaches beyond RNAi. Meanwhile, our results are highly consistent with the study by Du *et al.* (*23*) for EE expression and function of TrpA1 and are also consistent with the RNA sequencing data showing TrpA1 expression in EEs, but not ISCs (*38*–*40*). First, our *TrpA1-GFP* knock-in flies showed that endogenous TrpA1 in the midgut is expressed only in Pros^{+} EEs (Fig. 2A). Moreover, all five of our isoform specific-expression cassettes showed high levels of expression only in EEs (fig. S2). Second, although Xu *et al.* (*22*) reported that the TrpA1 agonist AITC could activate Ca^{2+} signals in ISCs/EBs, we found that AITC did not activate Ca^{2+} signals in ISCs/EBs (Fig. 2, B and C) in our preparation, while this same assay could activate Ca^{2+} signals in EEs. ISCs/EBs can respond to AITC stimulation in this assay if we expressed a *TrpA1* transgene in these cells, demonstrating that the AITC can access to ISCs/EBs. These results together indicate that TrpA1 expression in ISCs/EBs, if any, is low and below the GCaMP assay detection limit. Third, expression of RNAi against *TrpA1* under the EE drivers *Pros-Gal4* or *TKg-Gal4* was sufficient to reduce ISC proliferation (Fig. 4, F and G). Together, we conclude that at the least a major function of TrpA1 resides in EEs, not ISCs/EBs.

Loss of TrpA1 should cause changes of function within EEs, which, in turn, regulates ISC proliferation. While there is reduction of all cell types at day 40 of TrpA1 mutants, in young TrpA1-KO animals, the total number of ISCs/EBs is comparable to wild-type controls and there is already a marked Ca^{2+} oscillation reduction in ISCs/EBs (Fig. 6, A and B). Therefore, loss of shear stress sensing within EEs could prohibit the proliferation potential of ISCs in young animals, which, in turn, cause the gradual loss or less growth in the number of all cell types at old stage. EEs in flies and mammals are not essential for viability but regulate physiology and metabolism of the intestine and whole body (*34*, *44*). While the mechanism by which TrpA1 regulates Ca^{2+} in EEs and then modulates proliferation of ISCs is far from clear, previous reports have implicated a role of EEs in ISC proliferation and lipid metabolism in ECs. Depletion of all EEs in newly eclosed flies leads to reduced ISC proliferation, partly via the regulatory loop of TK in EEs and then Dilp3 expression in visceral muscle that, in turn, regulates insulin signaling in ISCs (*34*). Moreover, the neuroendocrine hormone Bursicon secreted by EEs represses the expression of the epidermal growth factor receptor ligand Vein in visceral muscle and thereby reduces ISC proliferation (*37*). It is important to note that EEs secrete a large array of peptides and hormones, and, therefore, complex and possibly opposite outcomes may occur when different genetic manipulations are conducted. Because Ca^{2+} signals are tightly linked to EE secretory functions (*56*), our results, nonetheless, suggest a possibility that shear stress elevates Ca^{2+} signals in EEs, leading to release of hormones and peptides that could further modulate ISC proliferation. It will be important for future studies to determine which hormones are released upon shear stress stimulation and how they might regulate Ca^{2+} oscillation and proliferation of ISCs.

TrpA1 has been shown to express at a high level in the enterochromaffin cells of mammalian gut (*57*). It is proposed that TrpA1 is activated by chemical components in the gut lumen to regulate serotonin release and gut motility. AITC has been shown to activate Ca^{2+} signals in enterochromaffin cells and stimulate serotonin release (*57*). As we have recently shown that mammalian TrpA1 behaves similarly to *Drosophila* TrpA1 by responding to shear stress (*24*), it will be of interest to determine whether enterochromaffin cells in mammals could sense shear stress through TrpA1 and, if so, whether shear stress sensing of enterochromaffin cells could play a role in gut growth and physiology.

MATERIALS AND METHODS

Drosophila stocks and transgenic lines

All fly stocks were raised on low yeast brown food, which was prepared by the University of Massachusetts Medical School *Drosophila* Resource Facility. Flies were maintained at room temperature, approximately 23°C, unless otherwise noted. For GCaMP imaging studies, 20-day-old adult female flies were used. For immunostaining studies, adult female flies were used at indicated age. The following fly strains were used in this study: *w*^{1118} (gift from P. Emery), *TrpA1-D-2A-Gal4* (*21*), *esg-Gal4* (BL#84324), *myo1A-Gal4* (*32*), *UAS-GCaMP6s* (BL#42746, BL#42749), *TrpA1-C-2A-Gal4* (*21*), *Pros-Gal4* (BL#84276), *TK-2A-Gal4* (BL#84693), *DH31-Gal4* (BL#51988), *TrpA1-GFP* (*21*), *AstA-2A-Gal4* (BL#84593), *AstC-2A-Gal4* (BL#84595), *CCHA1-2A-Gal4* (BL#84361), *CCHA2-2A-Gal4* (BL#84602), *CG30340-2A-Gal4* (BL#84611), *DH31-2A-Gal4* (BL#84623), *MIP-2A-Gal4* (BL#84651), *UAS-6XGFP* (BL#52262), *LexAop-6XmCherry* (BL#52267), *TrpA1-2A-Gal4* (*21*), *TrpA1-2A-LexA* (*21*), *UAS-luciferase-RNAi* (BL#31603), *UAS-TrpA1-RNAi* (BL#36780), *TrpA1-KO* (*21*), *R61H07-Gal4* (BL#39282), *UAS-TrpA1-A* (*21*), *UAS-TrpA1-D* (*21*), *UAS-TrpA1-D-E1017K* (*24*), *TrpA1-FLAG* (*21*), *Gr28b-LexA* (lab stock), *LexAOP-GCaMP6s* (BL#44589), *elav-Gal80* (lab stock), *TrpA1-A-KI* (*21*), *TrpA1-D-KI* (*21*), *UAS-EGFP-RNAi* (BL#41552), *UAS-mCherry.NLS* (BL#38425), and *tubP-Gal80*^{ts} (BL#7018).

Live Ca^{2+} imaging

Imaging was conducted under a Zeiss LSM700 upright confocal microscope with a 20×/1.0 numerical aperture water immersion objective. Throughout the studies, the genetically encoded Ca^{2+} indicator GCaMP6s was used to report the responses of cells. Ca^{2+} responses were defined as the maximum fluorescence fold change [$\Delta F/F_0 = (F - F_0)/F_0$], where F is the maximum Ca^{2+} signal value under certain stimulation condition and F_0 is the Ca^{2+} signal value right before the stimulation. Specific imaging parameters for each experiment were

listed in the following methods sections. Ca^{2+} signals were analyzed with ImageJ (National Institutes of Health).

Mechanical shear stress assay in microfluidic chamber

The microfluidic chamber (22 mm in length, 12 mm in width, and 200 μm in height) was fabricated using the standard soft lithography method. Polydimethylsiloxane solution (Sylgard 184, Dow Corning, Midland, MI) was poured over a customized channel mold and cured at 70°C for 2 hours to produce a negative replica of the channel. The inlet of the microfluidic chamber was connected to a syringe pump (PHD 2000, Harvard Instruments), which controlled the flow rate (fig. S1A). The shear stress (σ) magnitude of laminar flow in the chamber was calculated as $\sigma = 6Q\eta/(WH^2)$ (1), where Q is the flow rate, η is the dynamic viscosity of the saline, and W and H are the width and height of the chamber, respectively (*58*). The midgut was dissected from 20-day-old female flies in adult hemolymph–like (AHL) saline (*54*), which contains 108 mM NaCl, 5 mM KCl, 2 mM $CaCl_2$, 8.2 mM $MgCl_2$, 4 mM $NaHCO_3$, 1 mM NaH_2PO_4, 5 mM trehalose, 10 mM sucrose, and 5 mM Hepes with pH adjusted to 7.4. Then, the midgut was slightly stretched and pinned down in the central sample chamber of the microfluidic device (fig. S1B). Next, the posterior midgut was cut open with two sharp syringe needles, and the internal content was removed to expose the lumen side of midgut. Two "∩" shaped tungsten wires [inside diameter (ID) of 0.024 mm] were further used to fix and flatten the exposed region. The chamber was sealed with a 22 mm–by–50 mm cover glass (no. 1.5, Fisherbrand) and filled with AHL for further imaging studies. For Ca^{2+}-free condition, the $CaCl_2$ in imaging saline was removed, and 5 mM EGTA was further added. Shear stress was delivered from a direction perpendicular to the anterior-posterior axis of the midgut. The genetically encoded Ca^{2+} indicator GCaMP6s was used to determine responses of different midgut cell types. Ca^{2+} responses in midgut cells were imaged as a time lapse of 13 Z-stack images at a Z step of 2.5 μm and speed of ~5 s per stack. Ca^{2+} signals from three to five cells for each sample with most obvious responses were chosen for analysis in ImageJ. When measuring mechanical responses of ISCs/EBs, we chose cells with weak Ca^{2+} oscillations for analysis.

Mechanical stretch assay

To deliver tissue stretch stimulation, the midgut from 20-day-old female flies was dissected in AHL, and the posterior midgut was pinned down over a cavity (~650 μm in width; fig. S1D). A probe made from a staple pin (with flat sides) with a width of ~500 μm was used to press down the midgut over the cavity, which caused stretch of the posterior midgut. Displacement of the probe was controlled by the programmable micromanipulator (MP285, Sutter Instrument) at a speed of 6 mm/s. The posterior midgut was depressed by 500 μm and stretched to ~180% of its original length based on calculation. There was ~30% failure rate due to gut breakage by stretch. Imaging was focused on the region of posterior midgut at one shoulder of the cavity (dashed region in fig. S1D). Ca^{2+} responses in posterior midgut cells were imaged as a time lapse of 15 Z-stack images at a Z step of 2.5 μm and speed of ~6 s per stack. As ECs exhibit weak Ca^{2+} signals, it is difficult to identify the same cells before and after stretch. Therefore, we randomly picked one EC before and after stretch stimulations for analysis.

Mechanical compression assay

The midgut from 20-day-old female flies was dissected and exposed as described in the shear stress assay. To mimic the compression stimulation, we used an end fire polished glass probe (5 to 10 μm in diameter) to compress the midgut cells of interest (fig. S1E). The glass probe was mounted on a piezo actuator (PAS005, Thorlabs), which is driven by a stimulator (S88, The Grass Instrument). The compressive force was delivered at an angel of about 25° relative to the horizontal plane. Cells were compressed by a 10-μm displacement and then immediately released. Ca^{2+} responses in posterior midgut cells were imaged as a time lapse of 10 Z-stack images at a Z step of 2.5 μm and speed of 2 s per stack.

Shear stress stimulations of HEK293T cells

HEK293T cells were cultured in Dulbecco's modified Eagle's medium (10017CV, Corning) supplemented with 10% fetal bovine serum (F2442, Sigma-Aldrich), 2 mM L-glutamine (25030081, Gibco), 1 mM sodium pyruvate (11360070, Gibco), penicillin (100 U/ml), and streptomycin (100 μg/ml) (30002CI, Corning) at 37°C and 5% CO_2. Cells were grown on 22-mm square cover glass (7220401, Electron Microscopy Sciences) coated with 0.2% gelatin (G9391, Sigma-Aldrich). Transfection was done with 3 μg of polyethylenimine (239662, Polysciences) per 3.5-cm dish 1 day after plating. PcDNA3.1-TrpA1-A, pcDNA3.1-TrpA1-D, pcDNA3.1-TrpA1-D-E1017K, or pcDNA3.1-TrpA1-D-FLAG was cotransfected with pcDNA3.1-GCaMP6s and pcDNA3.1 empty vector into cells at a ratio of 0.05:0.4:0.55 (in micrograms) per 3.5-cm dish. GCaMP imaging was performed 2 days after transfection. Cells were allowed to habituate for 15 min at room temperature before experiments. Extra care was taken in handling the plates to minimize stimulation of the cells from shaking.

External imaging saline contained 130 mM NaCl, 3 mM KCl, 0.6 mM $MgCl_2$, 1 mM $CaCl_2$, 1.2 mM $NaHCO_3$, 10 mM glucose, and 10 mM Hepes with pH adjusted to 7.3. Shear stress stimulations were delivered horizontally through a glass micropipette (outer diameter, 1.2 mm; ID, 0.69 mm; Sutter Instrument) at 1 mm away from the center of the imaging field. Flow rate is controlled by a syringe pump (PHD 2000, Harvard Instruments), and shear stress response was tested at three levels (0.05, 0.25, and 1.25 dyne/cm^2) with a stepwise manner. Shear stress was calculated as $\sigma = 4\eta Q/(\pi r^3)$ (2) (*59*), where η is the viscosity of saline (the viscosity of water at room temperature, at a value of 1 mPa·s, was used), Q is the flow rate, $\pi = 3.14$, and r is the internal radius of the micropipette (345 μm). Time-lapse tracking of GCaMP6s signals was performed at 2.5 frames/s, and the mean value of GCaMP6s signals for each frame was quantified.

Ca^{2+} oscillations in ISCs/EBs

The guts from 20-day-old female flies were dissected, slightly stretched, and fixed at two ends with insect pins. For imaging the spontaneous Ca^{2+} oscillations in ISCs/EBs, GCaMP6s was expressed in ISCs/EBs with *esg-Gal4* to monitor the cytosolic Ca^{2+} changes. Meanwhile, all ISCs/EBs are also labeled by a nuclear marker, mCherry.NLS. Imaging was focused on posterior midgut. AHL saline was used for imaging. To reduce peristaltic movements of gut, isradipine (10 μg/ml) was added to imaging saline (*54*). Ca^{2+} signals were tracked as a time lapse of 17 Z-stack images at a Z step of 4 μm and speed of ~13.5 s per stack. Every gut will be tracked 10 min. The oscillating Ca^{2+} signals in ISCs/EBs flash like fireflies

(movies S1 to S3). Therefore, the number of cells with identifiable Ca^{2+} signals captured within each stack was counted manually, and the average number of captured oscillating cells across the 10 min tracking period was used for comparison.

Immunostaining

Whole guts from female w^{1118}, *TrpA1-FLAG*, and *TrpA1-KO* mutant (different days as specified in legend) were fixed in 4% paraformaldehyde (15710-S, Electron Microscopy Sciences) in phosphate-buffered saline (PBS) for 2 hours under room temperature. The following rinses, washes, and incubations with primary and secondary antibodies were in the 1× PBS containing 0.5% bovine serum albumin and 0.1% Triton X-100. The following primary antibodies were used: mouse anti-Pros [1:50, Developmental Studies Hybridoma Bank (DSHB)], mouse anti-armadillo (1:50, DSHB), rabbit anti–p-H3 (1:1000, Abcam), mouse FLAG-M2 (1:500, Sigma-Aldrich), goat anti-mouse immunoglobulin G (IgG) conjugated to Alexa 568 (1:1000, Invitrogen), and goat anti-rabbit IgG conjugated to Alexa 555 (1:1000, Invitrogen). The tissues were mounted in antifade medium with 4′,6-diamidino-2-phenylindole (VECTASHIELD, Vector Laboratories). Images were captured with Nikon Spinning Disk confocal microscope and processed using ImageJ.

Examination of midgut peristalsis

Adult female flies at 10/20/40 days old were first starved for 2 hours. Then, flies were transferred to vials with regular food containing 2.5% FD&C Blue #1 (FD110, Spectrum). After 10 or 30 min of feeding, the flies were anesthetized immediately on ice. The midguts were dissected out in PBS supplemented with 5 mM EGTA to block the peristalsis. The length of midgut with the dyed food, indicative of the food ingestion and peristalsis capability of midgut, was analyzed. This experiment is done at room temperature.

Paraquat feeding

Adult female flies at 5 days old were starved for 6 to 8 hours and then transferred to vials with regular food containing 2 mM paraquat (856177, Sigma-Aldrich). Then, the flies were kept in an incubator (I-36VL, Percival Scientific) with the temperature at 25°C and humidity at 60%. Midguts were dissected and immunostained after 3 days of paraquat feeding. The food was changed every day. The paraquat containing food was prepared freshly each day by mixing the paraquat powder in melted regular food.

Statistical analysis

Statistical analysis was performed using GraphPad Prism 7 software. Three or more experiments using individual biological samples were performed for each of the experimental results presented in this study. The n in each figure represents the number of midgut or cells counted under each experimental condition. For all statistics in this study, the error bar is SEM. The P value is presented as $^{*}P < 0.05$, $^{**}P < 0.01$, $^{***}P < 0.001$, and $^{****}P < 0.0001$. n.s. means not significant with $P > 0.05$.

Supplementary Materials

This PDF file includes:
Figs. S1 to S7
Legends for movies S1 to S3

Other Supplementary Material for this manuscript includes the following:
Movies S1 to S3

View/request a protocol for this paper from *Bio-protocol*.

REFERENCES AND NOTES

1. M. Krishnan, S. Kumar, L. J. Kangale, E. Ghigo, P. Abnave, The act of controlling adult stem cell dynamics: Insights from animal models. *Biomolecules* **11**, 667 (2021).
2. G. Mannino, C. Russo, G. Maugeri, G. Musumeci, N. Vicario, D. Tibullo, R. Giuffrida, R. Parenti, D. L. Furno, Adult stem cell niches for tissue homeostasis. *J. Cell. Physiol.* **237**, 239–257 (2022).
3. M. C. Funk, J. Zhou, M. Boutros, Ageing, metabolism and the intestine. *EMBO Rep.* **21**, e50047 (2020).
4. R. K. Zwick, B. Ohlstein, O. D. Klein, Intestinal renewal across the animal kingdom: Comparing stem cell activity in mouse and *Drosophila*. *Am. J. Physiol. Gastrointest. Liver Physiol.* **316**, G313–G322 (2019).
5. H. L. Larsen, K. B. Jensen, Reprogramming cellular identity during intestinal regeneration. *Curr. Opin. Genet. Dev.* **70**, 40–47 (2021).
6. R. Seishima, N. Barker, A contemporary snapshot of intestinal stem cells and their regulation. *Differentiation* **108**, 3–7 (2019).
7. Y. Hayakawa, H. Nakagawa, A. K. Rustgi, J. Que, T. C. Wang, Stem cells and origins of cancer in the upper gastrointestinal tract. *Cell Stem Cell* **28**, 1343–1361 (2021).
8. G. Zhu, J. Hu, R. Xi, The cellular niche for intestinal stem cells: A team effort. *Cell Regen.* **10**, 1 (2021).
9. B. Ohlstein, A. Spradling, The adult Drosophila posterior midgut is maintained by pluripotent stem cells. *Nature* **439**, 470–474 (2006).
10. C. A. Micchelli, N. Perrimon, Evidence that stem cells reside in the adult *Drosophila* midgut epithelium. *Nature* **439**, 475–479 (2006).
11. C. A. Duckworth, Identifying key regulators of the intestinal stem cell niche. *Biochem. Soc. Trans.* **49**, 2163–2176 (2021).
12. J. Yin, L. Sunuwar, M. Kasendra, H. Yu, C. M. Tse, C. C. Talbot Jr., T. Boronina, R. Cole, K. Karalis, M. Donowitz, Fluid shear stress enhances differentiation of jejunal human enteroids in intestine-chip. *Am. J. Physiol. Gastrointest. Liver Physiol.* **320**, G258–G271 (2021).
13. Q. Li, N. K. Nirala, Y. Nie, H. J. Chen, G. Ostroff, J. Mao, Q. Wang, L. Xu, Y. T. Ip, Ingestion of food particles regulates the mechanosensing misshapen-yorkie pathway in drosophila intestinal growth. *Dev. Cell* **45**, 433–449.e6 (2018).
14. S. W. Kim, J. Ehrman, M. R. Ahn, J. Kondo, A. A. M. Lopez, Y. S. Oh, X. H. Kim, S. W. Crawley, J. R. Goldenring, M. J. Tyska, E. C. Rericha, K. S. Lau, Shear stress induces noncanonical autophagy in intestinal epithelial monolayers. *Mol. Biol. Cell* **28**, 3043–3056 (2017).
15. L. He, G. Si, J. Huang, A. D. T. Samuel, N. Perrimon, Mechanical regulation of stem-cell differentiation by the stretch-activated Piezo channel. *Nature* **555**, 103–106 (2018).
16. C. Alcaino, K. R. Knutson, A. J. Treichel, G. Yildiz, P. R. Strege, D. R. Linden, J. H. Li, A. B. Leiter, J. H. Szurszewski, G. Farrugia, A. Beyder, A population of gut epithelial enterochromaffin cells is mechanosensitive and requires Piezo2 to convert force into serotonin release. *Proc. Natl. Acad. Sci. U.S.A.* **115**, E7632–E7641 (2018).
17. A. Mercado-Perez, A. Beyder, Gut feelings: Mechanosensing in the gastrointestinal tract. *Nat. Rev. Gastroenterol. Hepatol.* **19**, 283–296 (2022).
18. M. Kim, G. Heo, S. Y. Kim, Neural signalling of gut mechanosensation in ingestive and digestive processes. *Nat. Rev. Neurosci.* **23**, 135–156 (2022).
19. H. J. Kim, D. Huh, G. Hamilton, D. E. Ingber, Human gut-on-a-chip inhabited by microbial flora that experiences intestinal peristalsis-like motions and flow. *Lab Chip* **12**, 2165–2174 (2012).
20. A. Manolache, A. Babes, R. Madalina Babes, Mini-review: The nociceptive sensory functions of the polymodal receptor Transient Receptor Potential Ankyrin Type 1 (TRPA1). *Neurosci. Lett.* **764**, 136286 (2021).
21. P. Gu, J. Gong, Y. Shang, F. Wang, K. T. Ruppell, Z. Ma, A. E. Sheehan, M. R. Freeman, Y. Xiang, Polymodal nociception in *Drosophila* requires alternative splicing of TrpA1. *Curr. Biol.* **29**, 3961–3973.e6 (2019).
22. C. Xu, J. Luo, L. He, C. Montell, N. Perrimon, Oxidative stress induces stem cell proliferation via TRPA1/RyR-mediated Ca^{2+} signaling in the *Drosophila* midgut. *eLife* **6**, e22441 (2017).

23. E. J. Du, T. J. Ahn, I. Kwon, J. H. Lee, J. H. Park, S. H. Park, T. M. Kang, H. Cho, T. J. Kim, H. W. Kim, Y. Jun, H. J. Lee, Y. S. Lee, J. Y. Kwon, K. Kang, TrpA1 regulates defecation of food-borne pathogens under the control of the duox pathway. *PLOS Genet.* **12**, e1005773 (2016).
24. J. Gong, J. Chen, P. Gu, Y. Shang, K. T. Ruppell, Y. Yang, F. Wang, Q. Wen, Y. Xiang, Shear stress activates nociceptors to drive *Drosophila* mechanical nociception. *Neuron* **110**, 3727–3742.e8 (2022).
25. K. Talavera, J. B. Startek, J. Alvarez-Collazo, B. Boonen, Y. A. Alpizar, A. Sanchez, R. Naert, B. Nilius, Mammalian transient receptor potential TRPA1 channels: From structure to disease. *Physiol. Rev.* **100**, 725–803 (2020).
26. S. E. Murthy, A. E. Dubin, A. Patapoutian, Piezos thrive under pressure: Mechanically activated ion channels in health and disease. *Nat. Rev. Mol. Cell Biol.* **18**, 771–783 (2017).
27. P. Jin, L. Y. Jan, Y. N. Jan, Mechanosensitive ion channels: Structural features relevant to mechanotransduction mechanisms. *Annu. Rev. Neurosci.* **43**, 207–229 (2020).
28. D. Douguet, E. Honore, Mammalian mechanoelectrical transduction: Structure and function of force-gated ion channels. *Cell* **179**, 340–354 (2019).
29. T. W. Chen, T. J. Wardill, Y. Sun, S. R. Pulver, S. L. Renninger, A. Baohan, E. R. Schreiter, R. A. Kerr, M. B. Orger, V. Jayaraman, L. L. Looger, K. Svoboda, D. S. Kim, Ultrasensitive fluorescent proteins for imaging neuronal activity. *Nature* **499**, 295–300 (2013).
30. D. Wirtz, K. Konstantopoulos, P. C. Searson, The physics of cancer: The role of physical interactions and mechanical forces in metastasis. *Nat. Rev. Cancer* **11**, 512–522 (2011).
31. A. Linan-Rico, F. Ochoa-Cortes, A. Beyder, S. Soghomonyan, A. Zuleta-Alarcon, V. Coppola, F. L. Christofi, Mechanosensory signaling in enterochromaffin cells and 5-HT release: Potential implications for gut inflammation. *Front. Neurosci.* **10**, 564 (2016).
32. H. Jiang, P. H. Patel, A. Kohlmaier, M. O. Grenley, D. G. McEwen, B. A. Edgar, Cytokine/Jak/Stat signaling mediates regeneration and homeostasis in the Drosophila midgut. *Cell* **137**, 1343–1355 (2009).
33. B. Deng, Q. Li, X. Liu, Y. Cao, B. Li, Y. Qian, R. Xu, R. Mao, E. Zhou, W. Zhang, J. Huang, Y. Rao, Chemoconnectomics: Mapping chemical transmission in Drosophila. *Neuron* **101**, 876–893.e4 (2019).
34. A. Amcheslavsky, W. Song, Q. Li, Y. Nie, I. Bragatto, D. Ferrandon, N. Perrimon, Y. T. Ip, Enteroendocrine cells support intestinal stem-cell-mediated homeostasis in *Drosophila*. *Cell Rep.* **9**, 32–39 (2014).
35. W. Reiher, C. Shirras, J. Kahnt, S. Baumeister, R. E. Isaac, C. Wegener, Peptidomics and peptide hormone processing in the *Drosophila* midgut. *J. Proteome Res.* **10**, 1881–1892 (2011).
36. W. Song, J. A. Veenstra, N. Perrimon, Control of lipid metabolism by tachykinin in *Drosophila*. *Cell Rep.* **9**, 40–47 (2014).
37. A. Scopelliti, J. B. Cordero, F. Diao, K. Strathdee, B. H. White, O. J. Sansom, M. Vidal, Local control of intestinal stem cell homeostasis by enteroendocrine cells in the adult *Drosophila* midgut. *Curr. Biol.* **24**, 1199–1211 (2014).
38. D. Dutta, A. J. Dobson, P. L. Houtz, C. Glasser, J. Revah, J. Korzelius, P. H. Patel, B. A. Edgar, N. Buchon, Regional cell-specific transcriptome mapping reveals regulatory complexity in the adult *Drosophila* midgut. *Cell Rep.* **12**, 346–358 (2015).
39. R. J. Hung, Y. Hu, R. Kirchner, Y. Liu, C. Xu, A. Comjean, S. G. Tattikota, F. Li, W. Song, S. Ho Sui, N. Perrimon, A cell atlas of the adult *Drosophila* midgut. *Proc. Natl. Acad. Sci. U.S.A.* **117**, 1514–1523 (2020).
40. X. Guo, C. Yin, F. Yang, Y. Zhang, H. Huang, J. Wang, B. Deng, T. Cai, Y. Rao, R. Xi, The cellular diversity and transcription factor code of *Drosophila* enteroendocrine cells. *Cell Rep.* **29**, 4172–4185.e5 (2019).
41. D. P. Leader, S. A. Krause, A. Pandit, S. A. Davies, J. A. T. Dow, FlyAtlas 2: A new version of the *Drosophila melanogaster* expression atlas with RNA-Seq, miRNA-Seq and sex-specific data. *Nucleic Acids Res.* **46**, D809–D815 (2018).
42. J. B. Brown, N. Boley, R. Eisman, G. E. May, M. H. Stoiber, M. O. Duff, B. W. Booth, J. Wen, S. Park, A. M. Suzuki, K. H. Wan, C. Yu, D. Zhang, J. W. Carlson, L. Cherbas, B. D. Eads, D. Miller, K. Mockaitis, J. Roberts, C. A. Davis, E. Frise, A. S. Hammonds, S. Olson, S. Shenker, D. Sturgill, A. A. Samsonova, R. Weiszmann, G. Robinson, J. Hernandez, J. Andrews, P. J. Bickel, P. Carninci, P. Cherbas, T. R. Gingeras, R. A. Hoskins, T. C. Kaufman, E. C. Lai, B. Oliver, N. Perrimon, B. R. Graveley, S. E. Celniker, Diversity and dynamics of the *Drosophila* transcriptome. *Nature* **512**, 393–399 (2014).
43. L. J. Macpherson, A. E. Dubin, M. J. Evans, F. Marr, P. G. Schultz, B. F. Cravatt, A. Patapoutian, Noxious compounds activate TRPA1 ion channels through covalent modification of cysteines. *Nature* **445**, 541–545 (2007).
44. X. Guo, J. Lv, R. Xi, The specification and function of enteroendocrine cells in *Drosophila* and mammals: A comparative review. *FEBS J.* **289**, 4773–4796 (2022).
45. S. Jang, J. Chen, J. Choi, S. Y. Lim, H. Song, H. Choi, H. W. Kwon, M. S. Choi, J. Y. Kwon, Spatiotemporal organization of enteroendocrine peptide expression in *Drosophila*. *J. Neurogenet.* **35**, 387–398 (2021).
46. L. E. O'Brien, S. S. Soliman, X. Li, D. Bilder, Altered modes of stem cell division drive adaptive intestinal growth. *Cell* **147**, 603–614 (2011).
47. B. Biteau, C. E. Hochmuth, H. Jasper, JNK activity in somatic stem cells causes loss of tissue homeostasis in the aging *Drosophila* gut. *Cell Stem Cell* **3**, 442–455 (2008).
48. T. Lee, L. Luo, Mosaic analysis with a repressible cell marker for studies of gene function in neuronal morphogenesis. *Neuron* **22**, 451–461 (1999).
49. G. M. Story, A. M. Peier, A. J. Reeve, S. R. Eid, J. Mosbacher, T. R. Hricik, T. J. Earley, A. C. Hergarden, D. A. Andersson, S. W. Hwang, P. McIntyre, T. Jegla, S. Bevan, A. Patapoutian, ANKTM1, a TRP-like channel expressed in nociceptive neurons, is activated by cold temperatures. *Cell* **112**, 819–829 (2003).
50. F. N. Hamada, M. Rosenzweig, K. Kang, S. R. Pulver, A. Ghezzi, T. J. Jegla, P. A. Garrity, An internal thermal sensor controlling temperature preference in *Drosophila*. *Nature* **454**, 217–220 (2008).
51. K. Kang, S. R. Pulver, V. C. Panzano, E. C. Chang, L. C. Griffith, D. L. Theobald, P. A. Garrity, Analysis of *Drosophila* TRPA1 reveals an ancient origin for human chemical nociception. *Nature* **464**, 597–600 (2010).
52. L. Zhong, A. Bellemer, H. Yan, H. Ken, R. Jessica, R. Y. Hwang, G. S. Pitt, W. D. Tracey, Thermosensory and nonthermosensory isoforms of *Drosophila melanogaster* TRPA1 reveal heat-sensor domains of a thermoTRP channel. *Cell Rep.* **1**, 43–55 (2012).
53. M. Chatterjee, Y. T. Ip, Pathogenic stimulation of intestinal stem cell response in *Drosophila*. *J. Cell. Physiol.* **220**, 664–671 (2009).
54. H. Deng, A. A. Gerencser, H. Jasper, Signal integration by Ca^{2+} regulates intestinal stem-cell activity. *Nature* **528**, 212–217 (2015).
55. A. A. Kim, A. Nguyen, M. Marchetti, X. Du, D. J. Montell, B. L. Pruitt, L. E. O'Brien, Independently paced Ca^{2+} oscillations in progenitor and differentiated cells in an ex vivo epithelial organ. *J. Cell Sci.* **135**, jcs260249 (2022).
56. N. W. Bellono, J. R. Bayrer, D. B. Leitch, J. Castro, C. Zhang, T. A. O'Donnell, S. M. Brierley, H. A. Ingraham, D. Julius, Enterochromaffin cells are gut chemosensors that couple to sensory neural pathways. *Cell* **170**, 185–198.e16 (2017).
57. K. Nozawa, E. Kawabata-Shoda, H. Doihara, R. Kojima, H. Okada, S. Mochizuki, Y. Sano, K. Inamura, H. Matsushime, T. Koizumi, T. Yokoyama, H. Ito, TRPA1 regulates gastrointestinal motility through serotonin release from enterochromaffin cells. *Proc. Natl. Acad. Sci. U.S.A.* **106**, 3408–3413 (2009).
58. R. G. Bacabac, T. H. Smit, S. C. Cowin, J. J. Van Loon, F. T. Nieuwstadt, R. Heethaar, J. Klein-Nulend, Dynamic shear stress in parallel-plate flow chambers. *J. Biomech.* **38**, 159–167 (2005).
59. M. Cha, J. Ling, G. Y. Xu, J. G. Gu, Shear mechanical force induces an increase of intracellular Ca^{2+} in cultured Merkel cells prepared from rat vibrissal hair follicles. *J. Neurophysiol.* **106**, 460–469 (2011).

Acknowledgments: We thank the Perrimon lab for sharing reagents. Stocks were obtained from the Bloomington *Drosophila* Stock Center. **Funding:** This work is supported by the National Institutes of Health, grants R01DK136013 (Y.X.), DK083450 (Y.T.I.), and GM107457 (Y.T.I.); the Martina Stern Memorial Fund (Y.X.); and the Dan and Diane Riccio Fund for Neuroscience (Y.X. and Y.T.I.) **Author contributions:** Conceptualization: J.G., N.K.N., Y.T.I., and Y.X. Methodology: J.G., N.K.N., J.C., Q.W., and P.G. Investigation: J.G., N.K.N., and F.W. Visualization: J.G. and N.K.N. Supervision: Y.T.I. and Y.X. Writing—original draft: J.G., N.K.N.,. Y.T.I., and Y.X. Writing—review and editing: J.G., N.K.N., Y.T.I., and Y.X. **Competing interests:** The authors declare that they have no competing interests. **Data and materials availability:** All data needed to evaluate the conclusions in the paper are present in the paper and/or the Supplementary Materials.

Submitted 11 May 2022
Accepted 18 April 2023
Published 24 May 2023
10.1126/sciadv.adc9660